# X-Ray Extinction Theory in the Bragg Geometry

M. Kuriyama and G. G. Cohen
Center for Materials Science, National Bureau of Standards, Washington, D.C. 20234

Z. Naturforsch. **37a**, 465–473 (1982); received February 9, 1982

*Dedicated to Professor Dr. G. Hildebrandt on his 60th Birthday*

In view of the renewed interest in surface reflection x-ray topography, a unified theory for the Bragg geometry has been laid out to explain the different types of image formation from the scattering point of view. The means by which the photons "infiltrate" a real crystal have been studied. The theory suggests, for example, a mechanism for image contrast inversion in the Bragg geometry, and will also be found to be important in other topics of high current interest, such as x-ray standing wave surface analysis and x-ray inelastic scattering at the Bragg angle.

## 1. Introduction

Current analysis of x-ray topographs consists largely of the results of perfect crystal theory, because it is generally accepted that the dynamical diffraction theory for an imperfect crystal is too complicated to be of any assistance in image interpretation. Unfortunately, the dynamical diffraction theory for a perfect crystal relies upon ideal translational invariance, which yields a diffracted beam of perfectly uniform intensity. This beam is entirely free of precisely that fine structure which it is the goal to interpret. The usual solution to this problem has been to add on additional bits of theory concerning absorption, extinction, and mosaic structure, with varying degrees of success.

The present paper was undertaken to lay out the framework for a dynamical diffraction interpretation of diffraction by real crystals with varying local degrees of imperfection. The theory presents a unified treatment of the different mechanisms of image formation, and offers, for example, some insight into contrast inversion for the Bragg geometry. The results can easily be used qualitatively to interpret x-ray topographic images. With greater effort, a quantitative, and much deeper, analysis can be carried out.

An important feature of diffraction by a perfect crystal is that when a parallel incident beam is diffracted, the outgoing beam does not exhibit any angular divergence. In real crystals, the diffracted beams have considerable angular divergence around the Bragg angle. In fact, there has long been evidence of such line broadening by the recommended practice of placing the photographic plate in close proximity to the sample in order to reduce blurring and to ensure good contrast. The detailed analysis of real crystals will require [1, 2] that the in- and out-states be experimentally characterized.

Until very recently, it was time consuming to accumulate data with an x-ray optical system of adequate quality to perform such a characterization. The current availability of synchrotron radiation makes it possible and practical to prepare a nearly parallel incident x-ray beam, and to analyze the diffracted beam with the required degree of accuracy. With such resources, x-ray topography is currently being exploited to study realistic, thicker samples under static as well as real-time, environmental conditions [3]. In this setting, the present work may be quite timely.

The calculations begin with the intensity of a diffracted x-ray beam, as given by the modulus square of the scattering (or probability) amplitude:

$$\langle \boldsymbol{k}', \nu', \boldsymbol{R}';\ \text{out}\ |\, \boldsymbol{k}, \nu, \boldsymbol{R};\ \text{in}\rangle .$$

This amplitude depends on the scattering angle, on the incoming and outgoing polarization directions, $\nu$ and $\nu'$, and on the positions on the crystal surfaces where the beam enters and exits, $\boldsymbol{R}$ and $\boldsymbol{R}'$. In diffraction from a perfect crystal [4], the outgoing photon momentum, $\boldsymbol{k}'$, is uniquely connected to the incoming momentum $\boldsymbol{k}$. Thus, no angular resolution of the detection system is required. Furthermore, translational invariance guarantees that the positions $\boldsymbol{R}$ and $\boldsymbol{R}'$ have no significance. In diffraction by a real crystal, the outgoing beam has in-

Reprint requests to Dr. M. Kuriyama, Center for Materials Science, National Bureau of Standards, Washington D.C. 20234, USA.

0340-4811 / 82 / 0500-0465 $ 01.30/0. — Please order a reprint rather than making your own copy.

creased angular divergence compared to that of the incoming beam, and a determination of $\boldsymbol{R}$ and $\boldsymbol{R}'$ is indeed relevant. The detection system will now have to be capable of analyzing the angular distribution of the diffracted intensity and of pinpointing the position of the observation point with the desired accuray. The detailed analysis of a real crystal requires a set of topographs, taken over a range of angles in the neighborhood of the Bragg angle, because there is no unique way of characterizing an imperfection from a single image. The validity of this is underscored by the fact of contrast inversion, where one obtains topographic images with opposite contrast from the same imperfection, depending on the observation conditions.

A careful line broadening analysis is required to obtain detailed information on crystal imperfection from the observed intensity patterns. Compared to ordinary line broadening analysis, where the location of a scattering or diffraction source inside the crystal is not important, we emphasize that here the portion of the crystal volume which is participating in the diffraction is significant. A diffracting domain of atoms can be identified with each entrance and exit position on the crystal surface or surfaces (Figure 1). It is important to notice that the diffracting domain varies as the incident and observation angles change.

Using $\tau_H = (\boldsymbol{k}/\boldsymbol{k}')_z = \sin\theta_{in}/\sin\theta_{out}$, where $\theta_{in}$ and $\theta_{out}$ are the grazing incoming and outgoing angles, we define:

$$\xi = -\tfrac{1}{2}[(1-\tau_H)\,v(\boldsymbol{0}) - \tau_H\{(\boldsymbol{k}+\boldsymbol{H})^2 - \boldsymbol{k}^2\}] \quad \text{for the in-state } \boldsymbol{k} \tag{1.1}$$

and

$$\eta = -\tfrac{1}{2}[(1-\tau_H)\,v(\boldsymbol{0}) - \tau_H\{(\boldsymbol{k}'+\boldsymbol{H})^2 - \boldsymbol{k}^2\}] \quad \text{for the out-state } \boldsymbol{k}'. \tag{1.2}$$

As usual, the refractive index is related to $\Re\mathrm{e}[v(\boldsymbol{0})]$ and the absorption coefficient is related to $\Im\mathrm{m}[v(\boldsymbol{0})]$. Later, we will use the coordinates $\xi$ and $\eta$ in a convenient dimensionless form.

The scattering amplitude for a given diffracting domain of atoms is written [2, 5]

$$\langle \boldsymbol{k}', \nu', \boldsymbol{R}';\ \text{out} \mid \boldsymbol{k}, \nu, \boldsymbol{R};\ \text{in}\rangle = F(\xi)\,\delta_{\xi,\eta} + C(\boldsymbol{R}, \boldsymbol{R}')\,G(\xi, \eta)\,. \tag{1.3}$$

The first term describes mosaic contrast for both the reflection and the transmission geometries, and (for Laue geometry only) disruption images formed via the effective absorption coefficient. (The effective absorption coefficient is part of extinction contrast in the transmission geometry.) The second term describes extinction contrast for both the reflection and the transmission geometries.

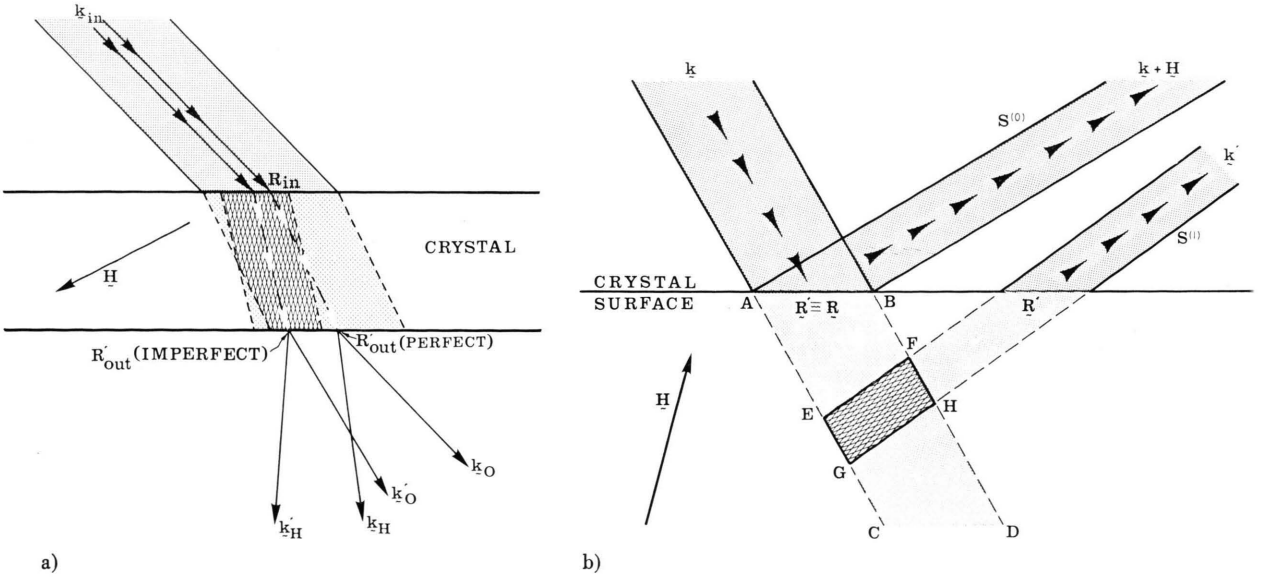


Fig. 1. a) Diffracting domain of atoms for a given incident beam and observation condition in the Laue geometry, where the domain is represented by the crosshatched area. The detector has a narrow spatial opening centered at $\boldsymbol{R}'$. b) Diffracting domain of atoms for the Bragg geometry.

As to the second term, it has been shown [6, 7] that $G(\xi, \eta)$ depends only weakly on $\eta$ in the transmission (Laue) geometry. However, we expect that $G$ depends strongly on both $\xi$ and $\eta$ for the surface reflection (Bragg) geometry. This effect has been seen [3, 8, 9, 10] in contrast reversal which takes place as the glancing angle changes, and it has also been seen [6, 7, 11] in the form of blurred images and images extending beyond the crystal edge.

The purpose of this paper is to revisit the physics of beam propagation within a crystal to understand which mode of the wave fields is activated, and to understand the role of absorption and scattering in this process. We emphasize dynamical absorption together with the scattering amplitude calculations, because separately a rigorous result is not achieved. The same theory will be found to be relevant to other topics of high current interest, such as inelastic scattering at the Bragg angle and x-ray standing wave surface analysis.

The basic equations for the real crystal are laid out in Section 2. Then the solutions for the "perfect" part are developed (Section 3) and the analogous solutions for the "imperfect" parts are given (Section 4). A discussion follows in Section 5, indicating the contribution that these methods can make to topography both at the present time and in the future.

## 2. Basic Equations for Dynamical Diffraction in Real Crystals

Dynamical diffraction in a real crystal, which has varying local degrees of perfection, can be described by two basic equations: the scattering amplitude equation and the particle Green's function equation. The former gives the amplitude of diffracted beams while the latter describes the propagation of particles (photons) inside the crystal. The scattering amplitude for an incoming beam with momentum $\boldsymbol{k}$ striking a crystal at $\boldsymbol{R}$ and emerging at $\boldsymbol{R}'$ with momentum $\boldsymbol{k}'$ can be written [1, 2] (with the polarization directions suppressed)

$$\begin{aligned}&\langle \boldsymbol{k}', \boldsymbol{R}';\ \text{out} \mid \boldsymbol{k}, \boldsymbol{R};\ \text{in}\rangle \\ &= \int \mathrm{d}^3p \int \mathrm{d}^3p'\, A^*(\boldsymbol{k}', \boldsymbol{p}';\ \boldsymbol{R}')\, S(\boldsymbol{p}', \boldsymbol{p}) \\ &\quad \cdot A(\boldsymbol{k}, \boldsymbol{p};\ \boldsymbol{R}),\end{aligned} \tag{2.1}$$

in terms of the scattering matrix element $S(\boldsymbol{p}', \boldsymbol{p})$, the spectral distribution $A$ for the incoming beam, and the detector response function $A^*$ for the outgoing beam. The $S$-matrix element is given by

$$\begin{aligned}S(\boldsymbol{p}', \boldsymbol{p}) = \delta(\boldsymbol{p}' - \boldsymbol{p}) + i \int_{\text{crystal}} \mathrm{d}^4x \int \mathrm{d}^4y\, f_{p'}^*(x) \\ \cdot [\Box_x \Box_y D(x, y) - (2\pi)^{-3} \\ \cdot \Box_y \delta(x - y)] f_p(y).\end{aligned} \tag{2.2}$$

The quantities $x$ and $y$ are four-vectors and the $\Box$'s are differential operators given by

$$\Box = \frac{1}{c^2} \frac{\partial^2}{\partial t^2} - \nabla^2$$

for x-rays and by $\Box = \varkappa(\partial/\partial t) - \nabla^2$ for electrons. The integral ranges are appropriately restricted to the crystal volume, and the function $f$ is written as a plane wave.

The particle Green's function $D(x, y)$ satisfies the second basic equation *inside* the crystal:

$$\begin{aligned}&\Box_x D(x, y) - \int \mathrm{d}^4x'\, \Gamma(x, x')\, D(x', y) \\ &= \delta(x - y),\end{aligned} \tag{2.3}$$

where $\Gamma(x, y)$ is the generalized polarizability (or the crystal potential) for imperfect crystals [2]. The properties of the generalized polarizability will be used later.

When (2.3) is solved, and the solution $D(x, y)$ is substituted into (2.2), the scattering amplitude of a crystal of arbitrary shape is obtained for a given beam geometry and its related diffracting domain of atoms. This process has been carried out [1, 2, 5] for diffraction topography in the Laue geometry. In this paper, the process will be repeated for the Bragg geometry, with emphasis on the distinctions between the two geometries. The scattering amplitude will be evaluated for an imperfect crystal of thickness $L$ in the $z$-direction, and of infinite extent in the other two orthogonal directions. The incident beam is of finite size, and its location at the entrance surface of the crystal is defined.

The Fourier transform of the generalized polarizability,

$$\begin{aligned}\Gamma(\boldsymbol{k}_1, \boldsymbol{k}_2) = \frac{1}{N} \sum_l v_l(\boldsymbol{k}_1, \boldsymbol{k}_2) \\ \cdot \exp[-i(\boldsymbol{k}_1 - \boldsymbol{k}_2) \cdot \boldsymbol{R}_l],\end{aligned} \tag{2.4}$$

will appear in the photon Green's function equation, where $N$ is the total number of atoms and $\boldsymbol{R}_l$ is the atomic position, displaced by $\boldsymbol{u}_l$ from the ideal lattice site $l$. The Fourier transform of the "atomic" polarizability for the $l$th atom is denoted by $v_l(\boldsymbol{k}_1, \boldsymbol{k}_2)$.

The vectors $\boldsymbol{k}_1$ and $\boldsymbol{k}_2$ represent the energy-momentum of the internal modes or the internal wave fields. In a natural approach, the formula for the scattering amplitude (2.1) would connect the energy-momentum $\boldsymbol{k}$ of the incoming beam to one of the variables, say $\boldsymbol{k}_2$, in the Fourier transform of the particle Green's function; and it would separately connect the energy-momentum $\boldsymbol{k}'$ of the outgoing beam to the other variable $\boldsymbol{k}_1$. The connection between $\boldsymbol{k}_1$ and $\boldsymbol{k}_2$ is determined through the polarizability equation (2.4). In other words one does not know whether a particular value of the outgoing $\boldsymbol{k}'$, in turn $\boldsymbol{k}_1$, has a non-vanishing scattering amplitude until one calculates to find a non-vanishing polarizability connecting this $\boldsymbol{k}_1$ to another particular value of $\boldsymbol{k}_2$, and in turn the incoming energy-momentum $\boldsymbol{k}$. This approach appears very complicated, but the calculation is unambiguous and straightforward. The reason we cannot use the traditional diffraction treatment, where $\boldsymbol{k}$ of the incoming beam is the only variable and $\boldsymbol{k}'$ is connected *a priori* to $\boldsymbol{k}$, is that this connection can only be made [1] for diffraction in a perfect crystal.

After substituting the solution of the photon Green's function equation (2.3), the scattering amplitude is obtained:

$$S(\boldsymbol{p}', \boldsymbol{p}) = \delta(\boldsymbol{p} - \boldsymbol{p}') + \frac{i}{2|\boldsymbol{p}|}\,\delta(|\boldsymbol{p}| - |\boldsymbol{p}'|)\sum_{\boldsymbol{I}}\sum_{\boldsymbol{q}_t}\delta(\boldsymbol{p}_t + \boldsymbol{I}_t + \boldsymbol{q}_t - \boldsymbol{p}_t')$$
$$\cdot\left[\{T_{+-}(\boldsymbol{I}) - T_{+0}(\boldsymbol{I})\}\exp\left[i(p_z + I_z - p_z')L\right] - T_{-0}(\boldsymbol{I}) + T_{00}(\boldsymbol{I})\right], \tag{2.5}$$

where

$$T_{\pm\pm}(\boldsymbol{I}) = (2p_z')(2p_z)\sum_{q_z}\int\frac{\mathrm{d}q_z'}{2\pi}\left\{[\mathbf{L}^{-1}(\boldsymbol{p})]_{\boldsymbol{I},\boldsymbol{0}}^{\boldsymbol{q},\boldsymbol{q}'} - \frac{1}{2p_z}\cdot\frac{1}{q_z'}\,\delta_{\boldsymbol{I},\boldsymbol{0}}\,\delta_{\boldsymbol{q},\boldsymbol{q}'}\right\}$$
$$\cdot\exp\left[\pm iq_z\cdot L\right]\exp\left[\pm iq_z'\cdot L\right]. \tag{2.6}$$

The $\pm$ subscripts on $T$ indicate the correct signs for the two exponentials, respectively. A zero subscript means that $L$ is set to zero in the appropriate exponential. The unit vector $\boldsymbol{t}$ is parallel to the crystal surfaces.

For each diffracting domain of atoms we can assign a particular perfect reference reciprocal lattice. It is natural to introduce $\mathbf{T}$ as a super-matrix (or a matrix of matrices) in order to treat both the local perfect reference crystal and the local imperfections contained in the diffracting domain. The vector $\boldsymbol{I}$ (and later also, $\boldsymbol{J}$ and $\boldsymbol{K}$) can take on the values of $\boldsymbol{0}$ or $\pm\boldsymbol{H}$, the reciprocal lattice vectors associated with the perfect reference crystal.

Since the diffracting domain of atoms may not consist entirely of a perfect crystal, the Fourier transform of the polarizability does not behave as a generalized Kronecker delta. The diffracted beams can appear in a broadened direction in the vicinity of the reciprocal lattice points $\boldsymbol{I}$ and $\boldsymbol{0}$. The deviations of the diffracted beams from the local ideal crystal are denoted by the vectors $\boldsymbol{q}$. (In the usual notation, $\boldsymbol{H} + \boldsymbol{q} = \boldsymbol{Q} = 4\pi\sin\theta/\lambda$.) Only the tangential components of $\boldsymbol{q}$, $\boldsymbol{q}_t$, have physical significance.

The quantity $\mathbf{L}^{-1}$ is the solution of the photon Green's function equation, expressed in matrix form. Although we will not derive the photon Green's function here, a brief description of the matrix $\mathbf{L}$ is given to elucidate the nature of dynamical diffraction in a real crystal. The photon Green's function equation (2.3) is written in its Fourier transform:

$$\mathbf{L}\cdot\boldsymbol{D} = \boldsymbol{E}, \tag{2.7}$$

where $\mathbf{L}$ is the Fourier transform of the operator $\Box - \Gamma$ in (2.3). $\boldsymbol{E}$ is a column vector consisting of the Fourier transform $\delta$-functions. One can write the matrix $\mathbf{L}$ as the sum of two matrices, $\mathbf{L}_0$ and $\mathbf{W}$, where $\mathbf{L}_0$ corresponds to the perfect reference crystal defined in the diffraction domain, and hence is a diagonal matrix with respect to $\boldsymbol{q}$ and $\boldsymbol{q}'$. $\mathbf{W}$ represents the crystal imperfection within this domain, and its matrix element is written

$$[W(\boldsymbol{l})]_{\boldsymbol{I},\boldsymbol{J}}^{\boldsymbol{q},\boldsymbol{q}'} = -\frac{1}{N}\sum_{\boldsymbol{l}} v_l(\boldsymbol{I} - \boldsymbol{J})\,\alpha_{\boldsymbol{I}-\boldsymbol{J}}(l)$$
$$\cdot\exp\left[-i(\boldsymbol{q} - \boldsymbol{q}')\boldsymbol{l}\right], \tag{2.8}$$

where

$$\alpha_{\boldsymbol{I}-\boldsymbol{J}}(l) = \exp\left[-i(\boldsymbol{I} - \boldsymbol{J})\cdot\boldsymbol{u}_l\right] - 1. \tag{2.9}$$

The form of $\mathbf{L}_0$ will be given explicitly in Sect. 3 for a single Bragg diffraction condition. The inverse

matrix $\mathbf{L}^{-1}$ is obtained from

$$\mathbf{L}^{-1} = \mathbf{L}_0^{-1} - \mathbf{L}_0^{-1}\mathbf{W}^{\mathrm{D}}\mathbf{L}_0^{-1}, \tag{2.10}$$

where the dynamical imperfection "potential" $\mathbf{W}^{\mathrm{D}}$ is calculated from $\mathbf{W}$. Corresponding to the first (perfect crystal) and second (imperfection) terms of $\mathbf{L}^{-1}$ the quantities given by (2.6) are now split into two terms:

$$T_{\pm\pm}(\boldsymbol{I}) = T_{\pm}^{(0)}(\boldsymbol{I}) + T_{\pm\pm}^{(1)}(\boldsymbol{I}). \tag{2.11}$$

## 3. The Bragg Geometry and the Laue Geometry

In this section, we will deal only with the perfect crystal. The first term of $\mathbf{T}$, corresponding to the perfect reference crystal, contains only the in-state, indicating that the in- and out-states are identical. This means that there is no angular divergence (i.e., $\boldsymbol{q}_{\mathrm{t}} = 0$) of the diffracted beams if the incoming beam is mathematically parallel.

In the Bragg geometry, only one surface of the crystal is involved, whereas in the Laue geometry, the entrance and exit surfaces of the crystal are different. This can be described by the asymmetry factor, $\tau_{\mathrm{H}}$, which is defined by

$$\tau_{\mathrm{H}} = \frac{\boldsymbol{k}_z}{\boldsymbol{k}'_z} = \frac{k_z}{(\boldsymbol{k}+\boldsymbol{H})_z}. \tag{3.1}$$

For simplicity, a single $\boldsymbol{H}$ Bragg diffraction is assumed, where the Fourier transforms of the polarizability, related to reciprocal lattice vectors $\mathbf{0}$, $\boldsymbol{H}$, and $-\boldsymbol{H}$, are non-vanishing:

$$[\mathbf{L}_0(\boldsymbol{p})]_{I,J}^{\boldsymbol{q},\boldsymbol{q}'} = \tag{3.2a}$$

$$\begin{pmatrix} h_0(\boldsymbol{q}_{\mathrm{t}}) + 2p_z q_z + q_z^2 & -v(-\boldsymbol{H}) \\ -v(\boldsymbol{H}) & h_{\mathrm{H}}(\boldsymbol{q}_{\mathrm{t}}) + (2p_z/\tau_{\mathrm{H}})q_z + q_z^2 \end{pmatrix},$$

where

$$h_I(\boldsymbol{q}_{\mathrm{t}}) = (\boldsymbol{p} + \boldsymbol{I} + \boldsymbol{q}_{\mathrm{t}})^2 - \boldsymbol{p}^2 - v(\mathbf{0}). \tag{3.2b}$$

The inverse of this matrix is given by

$$[\mathbf{L}_0^{-1}(\boldsymbol{p})]_{I,J}^{\boldsymbol{q},\boldsymbol{q}'} = \frac{1}{\det|\mathbf{L}_0|}\mathbf{A}(\boldsymbol{q}_{\mathrm{t}}, q_z), \tag{3.3}$$

where $\mathbf{A}$ is the adjoint matrix of $\mathbf{L}_0$ (see Ref. [12]). In the traditional method, the determinant of $\mathbf{L}_0$ is set equal to zero, yielding the dispersion equation. (For multiple diffraction cases, see Refs. [13] and [14].) In this approach, the scattering amplitude is given by the residues of the integrals, evaluated for the poles in the complex plane $q_z$, where these are also given by setting the determinant equal to zero.

*a) Back Scattering*

For a single Bragg diffraction, $\det|\mathbf{L}_0|$ is a quartic equation written,

$$\det|\mathbf{L}_0| = (q_z - \lambda_1)(q_z - \lambda_2)(q_z - \lambda_3)(q_z - \lambda_4).$$

Two of the $\lambda_i$'s correspond to backscattering modes, and the other two yield the traditional dynamical diffraction modes.

The variable $q_z$ can be very close to zero (i.e., there exist some modes which are very close to the free photon state). This is equivalent to saying that the tie points lie near the Ewald sphere. We will call these two modes $\lambda_1$ and $\lambda_2$. They are negligibly small compared to $\lambda_3$ and $\lambda_4$. Then,

$$\det|\mathbf{L}_0| \cong (q_z - \lambda_3)(q_z - \lambda_4)q_z^2.$$

Comparing this to the exact equation, we find

$$\begin{aligned}(q_z - \lambda_3)(q_z - \lambda_4)q_z^2 &= \left[q_z^2 + 2p_z\left(1 + \frac{1}{\tau_{\mathrm{H}}}\right)q_z \right. \\ &\quad \left. + \left\{h_0 + h_{\mathrm{H}} + \frac{(2p_z)^2}{H}\right\}\right]q_z^2. \end{aligned} \tag{3.4}$$

The function within the square brackets yields the values of $\lambda_3$ and $\lambda_4$ when it is set equal to zero.

The contribution of these two modes to the scattering amplitude is of the order of $(|v(\mathbf{0})|/k_z^2)^2$, and is negligible [1]. It would be interesting to test if these contributions are still negligible for extremely asymmetric diffraction or when the Bragg angle is almost $\pi/2$ (see [15—19]).

Since the backscattering solutions do not contribute significantly to the scattering amplitude for the common diffraction range, we can safely assume, for these cases, that the determinant of $\mathbf{L}_0$ is equal to $\lambda_3\lambda_4(q_z - \lambda_1)(q_z - \lambda_2)$. The effective $\det|\mathbf{L}_0|$ for these two modes is:

$$\begin{aligned}\det|\mathbf{L}_0| &= \frac{(2p_z)^2}{\tau_{\mathrm{H}}}(q_z - \lambda_1)(q_z - \lambda_2) \\ &= \frac{(2p_z)^2}{\tau_{\mathrm{H}}}q_z^2 + \frac{1}{\tau_{\mathrm{H}}}(h_0 + \tau_{\mathrm{H}}h_{\mathrm{H}}) \\ &\quad \cdot (2p_z)q_z + h_0 h_{\mathrm{H}} - v(\boldsymbol{H})v(-\boldsymbol{H}). \end{aligned} \tag{3.5}$$

The $\lambda_i$ for $i = 1$ and 2 are:

$$\lambda_i = \frac{1}{2k_z}[v(\mathbf{0}) + \eta + (-1)^i R(\eta)], \tag{3.6}$$

where

$$R(\eta) = \sqrt{\eta^2 + \tau_{\mathrm{H}}v(\boldsymbol{H})v(-\boldsymbol{H})}. \tag{3.7}$$

When $q_t$ is equal to zero, $\eta$ for the out-state becomes identical to $\xi$ for the in-state. The quantities $R$ and $\lambda_i$ are complex since $v(\pm \boldsymbol{H})$ and $v(\boldsymbol{0})$ are complex. The imaginary parts of $\lambda_i$ are shown in Fig. 2 for the Laue geometry and in Fig. 3b for the symmetrical Bragg geometry.

In the Laue geometry, under a single Bragg condition, the singularities are located in the same (upper) half of the complex momentum plane, because the linear absorption coefficient ($\Im\mathrm{m}[v(0)]$) is always positive [1]. For a particular contour of integration in the upper half of the plane, both singularities participate in the scattering, while for another contour in the lower half of the plane, neither of the singularities participate.

In contrast to this, the singularities for the Bragg geometry are found in both the upper and lower halves of the complex plane. Thus, the Bragg geometry always permits at least one singularity for any contour either in the upper or in the lower half of the complex plane. This situation leads to non-vanishing $T_{\pm}^{(0)}$ and $T_0^{(0)}$ integrals, resulting (in perfect crystals) to total reflection, independent of the crystal thickness.

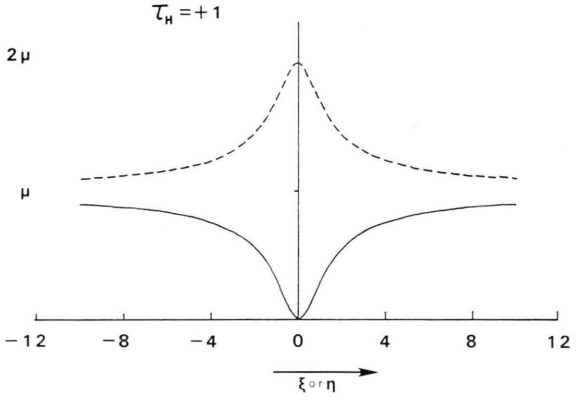


Fig. 2. $\Im\mathrm{m}[\lambda_i]$ for the Laue geometry. Mode 1 is given by the solid line and mode 2 by the dashed line.

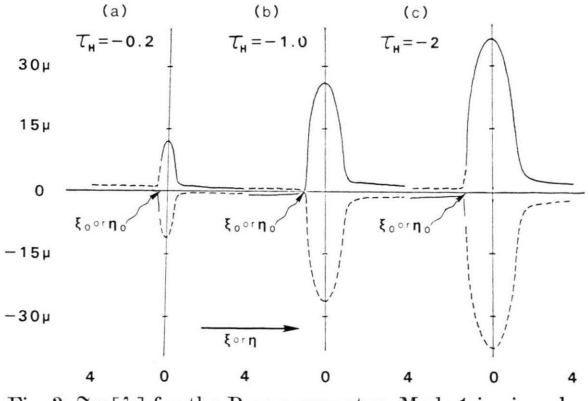


Fig. 3. $\Im\mathrm{m}[\lambda_i]$ for the Bragg geometry. Mode 1 is given by the solid line and mode 2 by the dashed line. a) magnifying mode; b) symmetrical diffraction; and c) demagnifying mode.

Also, in the Bragg geometry, there is a sign change in $\Im\mathrm{m}[\lambda_i]$ at $\xi_0$ and $\eta_0$. This indicates that there is a "mode flip" as the glancing angle $\xi$ and the observation angle $\eta$ change. The sign of the imaginary part of $\lambda_i$ determines in which half of the complex plane the singularity $\lambda_i$ appears, as a function of the coordinates $\xi$ and $\eta$. The calculated rocking curve (Fig. 4) shows that the left shoulder of the curve is derived from mode 2, whereas the top and the right shoulder come from mode 1. Physically, this mode flip causes image contrast reversal.

The imaginary part of the singularities is related to the absorption coefficient of the crystal, and the real part to the phase of the diffracted wave. The singularities in the Bragg geometry have an imaginary part that is directly proportional to the modulus of the atomic scattering power (the structure factor) instead of the atomic absorption coefficient (Laue geometry). The roles of the real and imaginary parts of the "wave vectors" are, so to speak, interchanged in going from one geometry over to

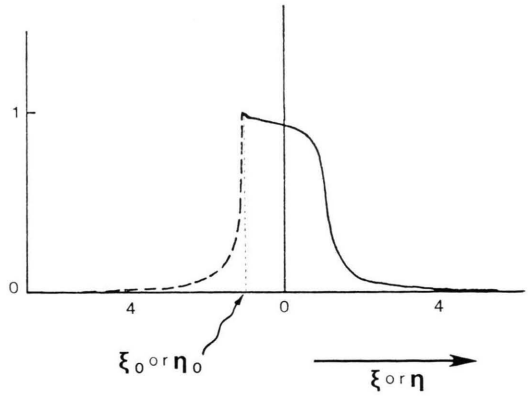


Fig. 4. Crystal rocking curve for the Bragg geometry, where the method of indicating the modes is the same as for Figs. 2 and 3. In all three figures (Fig. 2, 3 and 4), a dimensionless form of $\xi$ and $\eta$ has been used. These are derived by dividing the coordinates by the quantity

$$\Delta = |v_r(\boldsymbol{H})|\sqrt{1-\varkappa_H^2} \quad \text{where}$$
$$\varkappa_H = |v_i(\boldsymbol{H})|/|v_r(\boldsymbol{H})|,$$

and $v(\boldsymbol{H}) = v_r(\boldsymbol{H}) + iv_i(\boldsymbol{H})$. All of the calculations are for $\sigma$-polarized Cu K$\alpha_1$ incident on Si (111). To go over to $\pi$-polarization, $v(\boldsymbol{H})$ is simply replaced by $pv(\boldsymbol{H})$, where $p$ is the polarization factor.

the other. This goes hand-in-hand with the fact that the diffraction extinction distance (proportional to the reciprocal structure factor) has physical significance in the Bragg geometry, whereas the ordinary extinction distance (proportional to the reciprocal of the atomic absorption coefficient) is a factor in the Laue geometry.

*b) Propagators*

We now evaluate the scattering amplitude using complex contour integration (for a classical analog, see Ref. [12]). We note in passing that the evaluation of the second (the imperfect crystal) term of **T** will require the same mathematics as the evaluation of the first (perfect crystal) term since the contour integration of

$$\int_{-\infty}^{\infty} \frac{\mathrm{d}z}{2\pi} \frac{\mathbf{A}}{\det|\mathbf{L}_0|} \exp[\pm i z \Lambda]$$

is involved in both terms. The quantity $\Lambda$ can be $l_z$, $L - l_z$ or $L$. It is also interesting to notice that the conservation of photon momenta (wave vectors) parallel to the crystal surface is a natural consequence of the scattering amplitude calculation.

For the Laue geometry, the scattering amplitude corresponding to the first term is given by

$$S^{(0)}_{\mathrm{Laue}}(\boldsymbol{p}, \boldsymbol{p}') = \sum_{\boldsymbol{K}} \delta(\boldsymbol{p} + \boldsymbol{K} - \boldsymbol{p}')\, \tau_{\boldsymbol{K}} \cdot \sum_i D^{(i)}_{\boldsymbol{K},\boldsymbol{0}}(\xi) \exp[i \lambda_i(\xi) L], \tag{3.8}$$

where the propagators (i.e., $\mathbf{L}_0^{-1}$) are expressed as

$$\mathbf{D}^{(i)}(\xi) = \begin{pmatrix} \frac{1}{2}\left[1 - (-1)^i \frac{\xi}{R(\xi)}\right] & \frac{(-1)^i v(-\boldsymbol{H})}{R(\xi)} \\ \frac{(-1)^i v(\boldsymbol{H})}{R(\xi)} & \frac{1}{2}\left[1 + (-1)^i \frac{\xi}{R(\xi)}\right] \end{pmatrix} \tag{3.9}$$

and $\boldsymbol{K}$ takes on the value of $\boldsymbol{0}$ and $\boldsymbol{H}$.

From here to the end of this section, we deal only with our primary topic, the Bragg geometry. The evaluation of the **T** integrals for the Bragg geometry requires special consideration because the crystal is bounded and cannot be approximated by an infinite volume without at least one surface. The Fourier transform of the polarizability, even for a perfect crystal, is a function of two photon momenta, $\boldsymbol{k}$ and $\boldsymbol{k}'$. In the traditional treatment, one assumes that the Fourier transform depends on the difference of the two vectors, rather than on each of them independently. When the crystal is of infinite size, the non-vanishing Fourier transform appears only at $(\boldsymbol{k}' - \boldsymbol{k}) = \boldsymbol{K}$ (a reciprocal lattice vector), because the lattice sum gives the generalized Kronecker delta (i.e., the Laue interference function). This is no longer true when the crystal is of a finite size, leading to a non-vanishing Fourier transform in the neighborhood of the $\boldsymbol{K}$'s. The range of this neighborhood around the $\boldsymbol{K}$'s is normally very small, but in dynamical diffraction, even such a small deviation ($\boldsymbol{q}$) cannot be ignored.

Since the Fourier transform of the polarizability is a function of $\boldsymbol{k}$, the quantity $v(\boldsymbol{H})\, v(-\boldsymbol{H})$ in (3.6) and (3.7) is a function of $q_z$. Then, $q_z - \lambda_i$ in $\det|\mathbf{L}_0|$ is replaced by

$$q_z - \lambda_i = 1 + (-1)^i \frac{(\tau_{\mathrm{H}} \alpha)}{4 k_z} \frac{1}{R(\xi)} (q_z - \lambda_i^{(0)}),$$

where

$$\alpha = [\partial \{v(\boldsymbol{H})\, v(-\boldsymbol{H})\}/\partial q_z]_{\lambda_i^{(0)}},$$

and $\lambda_i^{(0)}$ is given by (3.6). This procedure yields the renormalization of propagators. For the evaluation of the **T** integrals, these renormalized $\det|\mathbf{L}_0|$ are used. Furthermore, we impose the condition that there should be no thickness independent contribution to the scattering amplitude for the incident beam. This condition leads to setting $(\tau_{\mathrm{H}} \alpha)/4 k_z$ to $-\xi$ or $-\eta$. What we have done here is to describe the physical process in which photons infiltrate the crystal by adjusting their momenta and the polarizability of the crystal.

We obtain

$$S^{(0)}_{\mathrm{Bragg}}(\boldsymbol{0}) = \delta(\boldsymbol{p} - \boldsymbol{p}') \{D^{(i)}_{\boldsymbol{0}\boldsymbol{0}}(\xi) \exp[i \lambda_i(\xi) L] - D^{(i+1)}_{\boldsymbol{0}\boldsymbol{0}}(\xi) \exp[-i \lambda_{i+1} L]\} \tag{3.10a}$$

for the 0-diffracted beam, and

$$S^{(0)}_{\mathrm{Bragg}}(\boldsymbol{H}) = \delta(\boldsymbol{p} + \boldsymbol{H} - \boldsymbol{p}') \cdot \{(-2) D^{(i)}_{\boldsymbol{H}\boldsymbol{0}}(\xi) + D^{(i)}_{\boldsymbol{H}\boldsymbol{0}}(\xi) \exp[i \lambda_i(\xi) L] - D^{(i+1)}_{\boldsymbol{H}\boldsymbol{0}}(\xi) \exp[-i \lambda_{i+1}(\xi) L]\} \tag{3.10b}$$

for the H-diffracted beam. Here, the propagators are given by:

$$D^{(i)}_{\boldsymbol{K}\boldsymbol{0}}(\xi) = \begin{pmatrix} \frac{1}{2}(-1)^i & \frac{1}{2}\left[\frac{R(\xi) + (-1)^i \xi}{v(\boldsymbol{H})}\right] \\ \frac{1}{2}\left[\frac{R(\xi) + (-1)^i \xi}{v(-\boldsymbol{H})}\right] & \frac{1}{2}\tau_{\mathrm{H}}\left[\frac{R(\xi) + (-1)^i \xi}{R(\xi) - (-1)^i \xi}\right] \end{pmatrix}. \tag{3.11}$$

The **T** integration tells us that the mode $i$ corresponds to the mode in which $\Im\mathfrak{m}[\lambda_i]$ is positive for a given range of $\xi$, while the mode $i+1$ has negative $\Im\mathfrak{m}[\lambda_{i+1}]$ for that range. The sign of $\Im\mathfrak{m}[\lambda_i]$ is the indicator by which the position of the mode flip is determined.

It is evident from Fig. 3 that the absolute value of $\Im\mathfrak{m}[\lambda_i]$ becomes very large as the glancing angle approaches the dynamical diffraction range. This means that the beam penetrates very little into the perfect crystal. The way in which this changes for asymmetric diffraction is shown in Figs. 3a and 3c.

The role of the **T** integration, as the indicator of the active mode, will become even more important for an imperfect crystal, as we show in the next section.

## 4. Imperfection Images in the Bragg Geometry

When the crystal is imperfect, the imperfections in the diffracting domain act as additional scatterers, creating extinction contrast in the diffracted beams. The second term of (2.11), the integral $\mathbf{T}^{(1)}$, contains $\mathbf{L}_0^{-1}$ twice. In effect, the $\mathbf{T}^{(1)}$ integral can be given as the product of two integral matrices. These integrals are identical to that for $\mathbf{T}^{(0)}$ except for the $\delta_{\boldsymbol{I},\mathbf{0}}$ term.

In imperfect crystals, the photon fields infiltrate the crystal until the fields encounter an imperfection which scatters photons. The scattered photons propagate within the crystal until they emerge from the crystal surface or are absorbed. The modes of the infiltration and the subsequent scattering are described by the appropriate propagators as determined by the $\mathbf{T}^{(1)}$ integration. Each propagator corresponds to a matrix element given by (3.11).

The scattering amplitude due to the imperfection is obtained as follows:

$$S^{(1)}(\boldsymbol{K}) = (iL/2p_z)\sum_{\boldsymbol{K}}\sum_{\boldsymbol{q}_t}(\boldsymbol{p}+\boldsymbol{K}+\boldsymbol{q}_t-\boldsymbol{p}')[\mathbf{T}^{(1)}]_{\boldsymbol{K}\mathbf{0}}, \tag{4.1}$$

where

I. for $\xi<\xi_0$ and $\eta<\eta_0$,

$$\mathbf{T}^{(1)} = (+1)\,\mathbf{D}^{(1)}(\eta)\,\mathbf{W}^{\mathrm{D}}\,\mathbf{D}^{(2)}(\xi)\cdot\exp[-i\{\lambda_1(\eta)-\lambda_2(\xi)\}l_z],$$

for $\xi<\xi_0$ and $\eta>\eta_0$,

$$\mathbf{T}^{(1)} = (-1)\,\mathbf{D}^{(2)}(\eta)\,\mathbf{W}^{\mathrm{D}}\,\mathbf{D}^{(2)}(\xi)\cdot\exp[-i\{\lambda_2(\eta)-\lambda_2(\xi)\}l_z],$$

or II. for $\xi>\xi_0$ and $\eta<\eta_0$,

$$\mathbf{T}^{(1)} = (-1)\,\mathbf{D}^{(1)}(\eta)\,\mathbf{W}^{\mathrm{D}}\,\mathbf{D}^{(1)}(\xi)\cdot\exp[-i\{\lambda_1(\eta)-\lambda_1(\xi)\}l_z],$$

for $\xi>\xi_0$ and $\eta>\eta_0$,

$$\mathbf{T}^{(1)} = (+1)\,\mathbf{D}^{(2)}(\eta)\,\mathbf{W}^{\mathrm{D}}\,\mathbf{D}^{(1)}(\xi)\cdot\exp[-i\{\lambda_2(\eta)-\lambda_1(\xi)\}l_z].$$

In actuality, $\mathbf{T}^{(1)}$ has additional thickness dependent terms, but these yield negligible contributions to **T**. The total scattering amplitude can thus be given by the sum of $S^{(0)}_{\mathrm{Bragg}}$ (3.10) and the above $S^{(1)}$. An important result is that, in the Bragg geometry, the signs shown for $\mathbf{T}^{(1)}$ describe image contrast reversal as a function of $\xi$ or $\eta$.

For comparison, we also display the Laue results. The Laue propagators are given by the matrix element of (3.9) instead of (3.11). The scattering amplitude is:

$$S_{\mathrm{Laue}}(K) = \tau_{\boldsymbol{K}}\,\delta(\boldsymbol{p}+\boldsymbol{K}-\boldsymbol{p}')\sum_i D^{(i)}_{\boldsymbol{K}\mathbf{0}}(\xi)\exp[+i\lambda_i(\xi)L] + (iL/2p_z)\,\delta(\boldsymbol{p}+\boldsymbol{K}+\boldsymbol{q}_t-\boldsymbol{p}')\cdot\sum_l\sum_{i,j}\sum_{\boldsymbol{I},\boldsymbol{J}} D^{(i)}_{\boldsymbol{K}\boldsymbol{I}}(\eta)\,[\mathbf{W}^{\mathrm{D}}(l)]_{\boldsymbol{I}\boldsymbol{J}}\,D^{(j)}_{\boldsymbol{J}\mathbf{0}}(\xi)\exp[+i\lambda_j(\xi)l_z]\exp[+i\lambda_i(\eta)(L-l_z)],$$

where $\Im\mathfrak{m}[\lambda_i]$ or $\Im\mathfrak{m}[\lambda_j]$ is positive. If one sums [6, 7] the first term and the $i=j$ part of the second term in $S_{\mathrm{Laue}}(K)$ above, a new first term can be written:

$$\sum_i D^{(i)}_{\boldsymbol{K}\mathbf{0}}\exp[-\mu^{(i)}_{\mathrm{eff}}L]\ \text{(times a phase factor)}.$$

The effective absorption coefficient, $\mu_{\mathrm{eff}}$, depends on the imperfection in the relevant diffracting domain of atoms.

## 5. Discussion

The intention of this paper is to present a method for the careful description of local imperfections within a sample crystal using in-and-out state diffractometry. We have sorted out the various contrast mechanisms according to their dependence on the in-state alone, or on their dependence on both the in- and out-states. Mosaic contrast is explained by the perfect reference crystal, defined in the dif-

fracting domain of atoms. Since this kind of contrast comes from the first term in the scattering amplitude, the imaging mechanism is entirely due to dynamical diffraction in a perfect crystal. No reduction in primary extinction is required; only the deviation of the glancing angle from the exact Bragg angle defined in the local perfect reference crystal plays a role.

In the Laue geometry, even this first term contains modifications due to crystal imperfections existing in the diffracting domain of atoms. Such modifications appear as an effective absorption coefficient, which is a function of the local imperfections.

Reduction of primary extinction shows up in the second term of the scattering amplitude. The dependence of the scattering amplitude on both the in-state and the out-state is more prominent in the Bragg geometry than in the Laue geometry. The effect appears as an increased divergence of the diffracted beams, in black and white images, and in contrast reversal as the incident angle or observation angle changes.

A comparison of Figs. 2 and 3b indicates that the beams infiltrate the crystal much less under diffraction in the Bragg geometry than the beams penetrate in the Laue geometry. (This is true even before considering the interaction of the modes in the Laue geometry which leads to anomalous transmission.) For asymmetric diffraction, the amount that the beam infiltrates the crystal appears to be greater for the magnifying case (Fig. 3a) and less for the demagnifying case (Figure 3c). A calculation of the rocking curve, using the same parameters as for Fig. 3b, leads to the picture shown in Figure 4. The sign of $\Im\mathrm{m}[\lambda_i]$ determines which mode is used. A topograph taken at an angle corresponding to a position on the left shoulder of the curve is expected to show different contrast from one taken from a position at the top or on the right shoulder. It should be obvious that contrast inversion can only be seen using nearly parallel incident beams because angular averaging would smear the effect.

We have emphasized that a set of topographs is required for the detailed interpretation of images produced by x-ray diffraction by real crystals. There are many situations, however, where such a detailed study is either not required or not possible. For example, the direction and magnitude of dislocation vectors, or the determination of active slip systems, can be obtained from pairs of Berg-Barrett topographs using different $\boldsymbol{H}$ diffracting planes. White beam topography is particularly suited to the early detection of a crystal grain newly formed from the melt. Also, it will not be straightforward to obtain sets of topographs where a real-time environmental study is underway. In these examples, the relevant results are accessible through a simplified application of the theory presented here. On the other hand, for microstructural characterization involving detailed structural modelling or the mapping of strains within a sample, the analysis presented here should prove to be very useful.

Looking to the future, when it may be possible to provide a collective description of imperfections, by means of a general local structure factor $\mathbf{W}^{\mathrm{D}}$, this method will be much easier to apply in a general line broadening context.

*Acknowledgement*

One of the authors (G. G. Cohen) gratefully acknowledges support while at Vassar College, where a portion of this work was undertaken, from the National Science Foundation under Grant No. DMR-78 10308.

[1] M. Ashkin and M. Kuriyama, J. Phys. Soc. Japan **21**, 1549 (1966).
[2] M. Kuriyama, J. Phys. Soc. Japan **23**, 1369 (1967).
[3] M. Kuriyama, W. J. Boettinger, and G. G. Cohen, Ann. Rev. of Mat' l Sci. **12**, 23 (1982).
[4] B. W. Batterman and H. Cole, Rev. Mod. Phys. **36**, 681 (1964).
[5] M. Kuriyama, J. Phys. Soc. Japan **25**, 846 (1968).
[6] M. Kuriyama, Acta Cryst. **A25**, 682 (1969).
[7] M. Kuriyama, W. J. Boettinger, and H. E. Burdette, Advances in X-Ray Analysis, **20**, 245 (1977).
[8] U. Bonse, Z. Phys. **153**, 278 (1958).
[9] M. Renninger, Z. Angew. Phys. **19**, 20 (1965).
[10] J. Gronkowski, Phys. Stat. Sol. **(a) 571**, 105 (1980).
[11] W. J. Spencer, Appl. Phys. Letters **2**, 133 (1963).
[12] M. Kuriyama, Acta Cryst. **A31**, 774 (1975).
[13] G. Hildebrandt, Phys. Stat. Sol. **24**, 245 (1967).
[14] B. Post, Phys. Rev. Lett. **39**, 760 (1977).
[15] P. Farwig and H. Schürmann, Z. Phys. **204**, 489 (1967).
[16] S. Kishino and K. Kohra, Japan. J. Appl. Phys. **10**, 551 (1971).
[17] T. Bedynska, Phys. Stat. Sol. **A19**, 365 (1973).
[18] J. Härtwig, Acta Cryst. **A37**, 802 (1981).
[19] S. L. Chang, Appl. Phys. Lett. **39**, 816 (1981).